

# A multi-technique search for year-scale $\gamma$ -ray quasi-periodic modulation in the high-redshift FSRQ PKS 2052–47

Sikandar Akbar<sup>a,\*</sup>

<sup>a</sup>Department of Physics University of Kashmir Srinagar 190006 India

## Abstract

We investigate long-timescale quasi-periodic oscillations in the  $\gamma$ -ray emission of the high-redshift flat-spectrum radio quasar PKS 2052–47 using monthly binned *Fermi*-LAT data spanning MJD 54727.99–58507.99. To assess the statistical significance of periodic features embedded in red-noise-dominated variability, we employ several complementary timing techniques, including the Lomb–Scargle periodogram, weighted wavelet Z-transform, date-compensated discrete Fourier transform, REDFIT assuming an AR(1) process, and damped random walk modelling. Taken together, the analyses reveal a dominant quasi-periodic modulation on a timescale of  $\sim 600$ –630 d, together with a secondary longer-timescale feature near  $\sim 1050$ –1110 d. Monte Carlo simulations demonstrate that the shorter-period signal exceeds the highest local confidence levels, while the longer modulation reaches  $\gtrsim 99$  per cent local significance in several tests; independent DRW-based simulations further show that both peaks rise above the  $4\sigma$  confidence envelope in the LSP analysis. Spectral-window diagnostics indicate that the detected periodicities are not artefacts of uneven sampling. A sliding-window analysis further shows that the QPO power varies with time, implying episodic rather than persistent modulation across the  $\sim 11$  yr baseline. We discuss possible physical interpretations in terms of geometric modulation of Doppler boosting associated with jet precession or helical structures, accretion-driven instabilities at the jet base, and SMBBH-induced dynamics. The presence of two timescales and their intermittent behaviour may reflect coupled geometric processes or near-resonant modulation patterns. Our results identify PKS 2052–47 as a promising case of long-timescale  $\gamma$ -ray QPOs and motivate future broadband spectral modelling and coordinated multiwavelength observations to test SMBBH scenarios and to determine the physical origin of the oscillations.

**Keywords:** galaxies: BL Lacertae objects: PKS 2052–47 - galaxies: jets - radiation mechanisms: non-thermal - gamma-rays: galaxies.

## 1. Introduction

The source PKS 2052–47 (also known as 4FGL J2056.2–4714) is a  $\gamma$ -ray-bright flat-spectrum radio quasar located at a redshift of  $z = 1.489$  (Jauncey et al., 1984). Early ATCA radio imaging and *Chandra* observations revealed a two-sided kiloparsec-scale jet with no extended X-ray emission (Marshall et al., 2005). Very-long-baseline interferometry observations from the TANAMI programme show that the parsec-scale structure is extremely compact, with a high brightness-temperature core of  $\sim 2 \times 10^{12}$  K and only a very faint jet component detected at 8.4 GHz (Kadler et al., 2007; Boeck et al., 2009). These properties establish PKS 2052–47 as a classical, strongly Doppler-boosted FSRQ.

PKS 2052–47 entered a phase of enhanced activity in mid-2009, when a prominent optical flare was reported by the Automatic Telescope for Optical Monitoring (ATOM; ATel #2158). Following a gradual bright-

ening since July 2009, the source reached a peak magnitude of  $R \simeq 15.6$  in August, representing the highest optical flux measured for this object by ATOM up to that time (Hauser et al., 2009). Shortly thereafter, the *Fermi* Large Area Telescope (LAT) reported a strong enhancement in  $\gamma$ -ray emission above 100 MeV, establishing a close temporal association between the optical outburst and high-energy activity (ATel #2160; Chang (2009)). On 2009 August 9, the source reached  $F(E > 100 \text{ MeV}) = (8.7 \pm 1.6) \times 10^{-7} \text{ ph cm}^{-2} \text{ s}^{-1}$  (statistical uncertainty only), approximately a factor of four above the average level observed during the preceding week (2009 July 29–August 4), confirming PKS 2052–47 as a highly variable  $\gamma$ -ray emitter.

Motivated by this activity, a coordinated multiwavelength campaign was conducted in September 2009, covering radio, sub-millimeter, optical/UV, X-ray, and  $\gamma$ -ray bands. *Swift*-XRT observations revealed a hard X-ray spectrum well described by an absorbed power-law model with a photon index of  $\Gamma_X \approx 1.5$ , while contemporaneous *Fermi*-LAT data showed a gradual rise in  $\gamma$ -ray flux leading into the flaring phase. The re-

\*Corresponding author: Sikandar Akbar  
Email address: darprince46@gmail.com (Sikandar Akbar)

sulting broadband spectral energy distribution (SED), constructed from quasi-simultaneous observations, displayed the characteristic double-humped blazar structure. The inverse-Compton component was found to dominate over the synchrotron peak, consistent with earlier historical SEDs and indicating that high-energy emission is primarily produced through inverse-Compton scattering processes (Chang et al., 2010).

Subsequent observations demonstrated that PKS 2052–47 has remained intermittently active throughout the *Fermi* era. In March 2020, the source again exhibited enhanced  $\gamma$ -ray emission, with the daily averaged flux above 100 MeV reaching  $F(E > 100 \text{ MeV}) \simeq 1.2 \times 10^{-6} \text{ ph cm}^{-2} \text{ s}^{-1}$ , nearly an order of magnitude higher than the long-term average reported in the fourth *Fermi*-LAT catalog (ATel #13541; Buson and Angioni 2020). During this episode, the photon index was  $\Gamma_\gamma = 2.3 \pm 0.2$ , consistent with the catalog value, indicating that the variability was dominated by flux changes rather than strong spectral-shape variations.

In addition to episodic flaring, PKS 2052–47 has been identified as a candidate source exhibiting long-term quasi-periodic variability in  $\gamma$  rays. A systematic all-sky search for cyclic  $\gamma$ -ray emission using *Fermi*-LAT data revealed a statistically significant quasi-periodic modulation with a characteristic period of  $\sim 640$  d, detected at high significance against white noise and remaining significant after accounting for red-noise processes (Prokhorov and Moraghan, 2017). A refined likelihood analysis yielded a consistent period of  $\sim 642$  d, significant at  $> 5\sigma$  against white noise and with only a  $\sim 0.4$  per cent probability of arising from a power-law noise spectrum (Prokhorov and Moraghan, 2017). Over the LAT baseline considered in that study, this corresponds to approximately 4.5 modulation cycles. Importantly, PKS 2052–47 belongs to a small group of high-redshift ( $z = 1.49$ ) blazars showing indication for quasi-periodic behaviour, making it particularly interesting in the context of long-term jet-modulation or binary supermassive black hole (SMBH) scenarios.

In this work, we present a comprehensive study of PKS 2052–47 based on long-term time-domain analysis of its *Fermi*-LAT  $\gamma$ -ray light curves. We perform an independent and dedicated search for quasi-periodic oscillation (QPO) signatures, applying rigorous significance tests and explicitly accounting for stochastic variability processes. We apply multiple time-series techniques—including Lomb–Scargle periodograms (LSP), weighted wavelet Z-transforms (WWZ), phase-folding analysis, first-order autoregressive modelling (REDFIT), date-compensated discrete Fourier transform (DCDFT), and damped random walk (DRW) simulations—to assess the consistency and temporal stability of the candidate QPO signals. Our goal is to place the periodicity claims on a statistically sound footing while accounting for red noise, uneven sampling, and finite-duration effects. The results critically test the periodicity hypothesis

for PKS 2052–47 and provide a general framework for future investigations of similar blazar candidates.

The structure of this paper is as follows: Section 2 describes the data selection and reduction. Section 3 presents the results of various time-series analyses applied to the  $\gamma$ -ray light curve. Section 4 presents the statistical significance assessment of the detected QPOs. Section 5 examines the temporal evolution of the detected QPOs. Finally, Section 6 summarizes the findings and discusses their physical implications.

## 2. Observations and Data reduction

### 2.1. *Fermi*-LAT

The *Fermi* Large Area Telescope (*Fermi*-LAT), aboard the *Fermi* Gamma-ray Space Telescope (formerly GLAST), is a space-based high-energy instrument launched in 2008. With a field of view of  $\sim 2.3$  sr, the LAT operates predominantly in sky-survey mode, providing complete coverage of the  $\sim 20$  MeV–500 GeV energy range every  $\sim 3$  h (Atwood et al., 2009). The LAT data were processed using the FermiTools software package (version 2.2.0) distributed by the Fermi Science Support Center (FSSC). Standard event selections and quality cuts were applied following the recommendations in the official LAT analysis documentation.<sup>1</sup> Photon events belonging to the SOURCE class (evclass=128, evtype=3) were extracted from a circular region of interest (ROI) of radius  $15^\circ$  centred on the target, together with a zenith-angle cut of  $90^\circ$  to suppress contamination from Earth-limb  $\gamma$  rays. Spectral analyses were carried out in the 0.1–300 GeV band, and an independent likelihood analysis was performed with the FERMIPY package (v1.0.1; Wood et al. 2017). The Galactic diffuse emission was described using the template gll\_iem\_v07.fits, while the isotropic background component was modeled with iso\_P8R3\_SOURCE\_V3\_v1.txt. The post-launch instrument response function P8R3\_SOURCE\_V3 was adopted throughout. Our source model included all objects from the fourth *Fermi*-LAT catalog (4FGL) located within  $25^\circ$  of the ROI centre. The normalizations of sources lying within  $10^\circ$  were allowed to vary during the likelihood fit, whereas more distant sources were fixed at their catalog values. For PKS 2052–47, both the flux normalization and spectral-shape parameters ( $\alpha$  and  $\beta$ ) were left free. A monthly binned  $\gamma$ -ray light curve was generated for the source. The analysis covered the interval MJD 54727.99–58507.99, corresponding to the first  $\sim 11$  yr of *Fermi*-LAT operations and encompassing the multiple activity states relevant for the QPO search.

## 3. Quasi-periodic oscillation

To search for quasi-periodic signatures in the  $\gamma$ -ray light curve of PKS 2052–47, we applied a range of com-

<sup>1</sup><https://fermi.gsfc.nasa.gov/ssc/data/analysis/>

plementary time-series analysis methods. These comprise the LSP, WWZ, REDFIT, DCDFT, and DRW modelling. In addition, extensive Monte Carlo simulations were carried out to evaluate the statistical significance of the identified features. The methodologies and their associated results are described in detail in the sections that follow.

### 3.1. Lomb-Scargle Periodogram (LSP)

The Lomb-Scargle periodogram (LSP) is a widely used technique for identifying periodic signals in unevenly sampled time-series data (Lomb, 1976; Scargle, 1982). Owing to its suitability for irregularly spaced light curves, it has become a standard tool in astronomical variability analyses. In this work, we employed the ASTROPY implementation of the Lomb-Scargle algorithm<sup>2</sup>, incorporating the measured flux uncertainties to improve the stability of the resulting periodograms. Our application of the LSP follows the approach adopted in our earlier variability studies (Akbar et al., 2025; Nazir et al., 2026). The frequency search was restricted to the range  $f_{\min} = 1/T$  to  $f_{\max} = 1/(2\Delta T)$ , where  $T$  denotes the total temporal baseline and  $\Delta T$  the characteristic sampling interval; further details of the underlying formalism are given by VanderPlas (2018).

The periodogram reveals two prominent peaks at frequencies of  $0.000920 \pm 0.000068 \text{ d}^{-1}$  and  $0.001655 \pm 0.000064 \text{ d}^{-1}$ , corresponding to periods of  $1087.2 \pm 80.4 \text{ d}$  and  $604.2 \pm 23.4 \text{ d}$ , respectively (panel (a) of Figure 1). The uncertainties on the inferred periods were estimated by fitting Gaussian profiles to the periodogram peaks and adopting the corresponding half-width at half-maximum (HWHM) as the error measure (VanderPlas, 2018; Akbar et al., 2025). To further examine these modulations, we constructed phase-folded  $\gamma$ -ray light curves using the two LSP periods and fitted them with sinusoidal models. The resulting folded profiles display coherent variations over multiple cycles, supporting the quasi-periodic nature of the emission. For visual clarity, two full cycles are shown in each panel (see panels (c) and (d) of Figure 1).

To further examine the stability of these features, we computed the generalized Lomb-Scargle periodogram (GLSP), which explicitly accounts for measurement uncertainties. The GLSP results are consistent with those obtained from the standard LSP, lending additional support to the presence of these candidate periodicities. To evaluate the statistical significance of the detected periodicities, we employed the `LombScargle.false_alarm_probability()` routine from the `astropy.timeseries` module with `method="baluev"`, which provides an analytic approximation of the false-alarm probability (FAP). This approach is based on the formalism developed by Baluev (2008), which uses

extreme-value statistics to estimate the FAP while accounting for the effective number of trials across the scanned frequency range. The number of independent frequencies,  $N_{\text{ind}}$ , is internally inferred from the time sampling, frequency grid, and total temporal baseline, and therefore does not need to be specified explicitly. This method yields a statistically grounded estimate of the probability that a given peak in the periodogram arises from stochastic fluctuations, enabling a quantitative assessment of its significance.

### 3.2. Weighted Wavelet Z-Transform (WWZ)

The weighted wavelet Z-transform (WWZ; Foster 1996) maps an unevenly sampled time series simultaneously into the time and frequency domains by convolving the light curve with a localized oscillatory kernel. This approach is particularly well suited for identifying transient or evolving periodicities, as it provides information on both the characteristic timescale and the epoch over which a given modulation is present. In addition, the WWZ power is expected to diminish when the periodic component becomes weaker, allowing changes in the strength of the signal with time to be tracked.

For the present study, we employed the abbreviated Morlet kernel, defined as

$$f[\omega(t - \tau)] = \exp \left[ i\omega(t - \tau) - c\omega^2(t - \tau)^2 \right], \quad (1)$$

with the corresponding WWZ projection

$$W[\omega, \tau : x(t)] = \omega^{1/2} \int x(t) f^*[\omega(t - \tau)] dt, \quad (2)$$

where  $f^*$  is the complex conjugate of the kernel,  $\omega$  denotes the angular frequency, and  $\tau$  is the temporal offset. The analysis was performed using the publicly available Python implementation of the WWZ algorithm<sup>3</sup>.

The resulting WWZ power distribution exhibits a dominant peak at  $0.001606 \pm 0.000110 \text{ d}^{-1}$  and a secondary longer-timescale feature at  $0.000947 \pm 0.000100 \text{ d}^{-1}$ , corresponding to periods of  $622.70 \pm 42.94 \text{ d}$  and  $1055.62 \pm 112.33 \text{ d}$ , respectively. Uncertainties on the inferred periods were obtained by fitting Gaussian profiles to the peaks in the average WWZ spectrum.

### 3.3. First-order Autoregressive Process (REDFIT)

AGN light curves, including those of blazars, are typically characterized by red-noise variability driven by stochastic processes in the jet or accretion disc. Such behaviour can be represented by a first-order autoregressive [AR(1)] model, in which the emission at a given epoch depends linearly on the immediately preceding value (Schulz and Mudelsee, 2002). This can be expressed as  $r(t_i) = A r(t_{i-1}) + \epsilon(t_i)$ , where  $A = \exp[-(t_i - t_{i-1})/\tau]$

<sup>2</sup><https://docs.astropy.org/en/stable/timeseries/lombscargle.html>

<sup>3</sup><https://github.com/eaydin/WWZ>

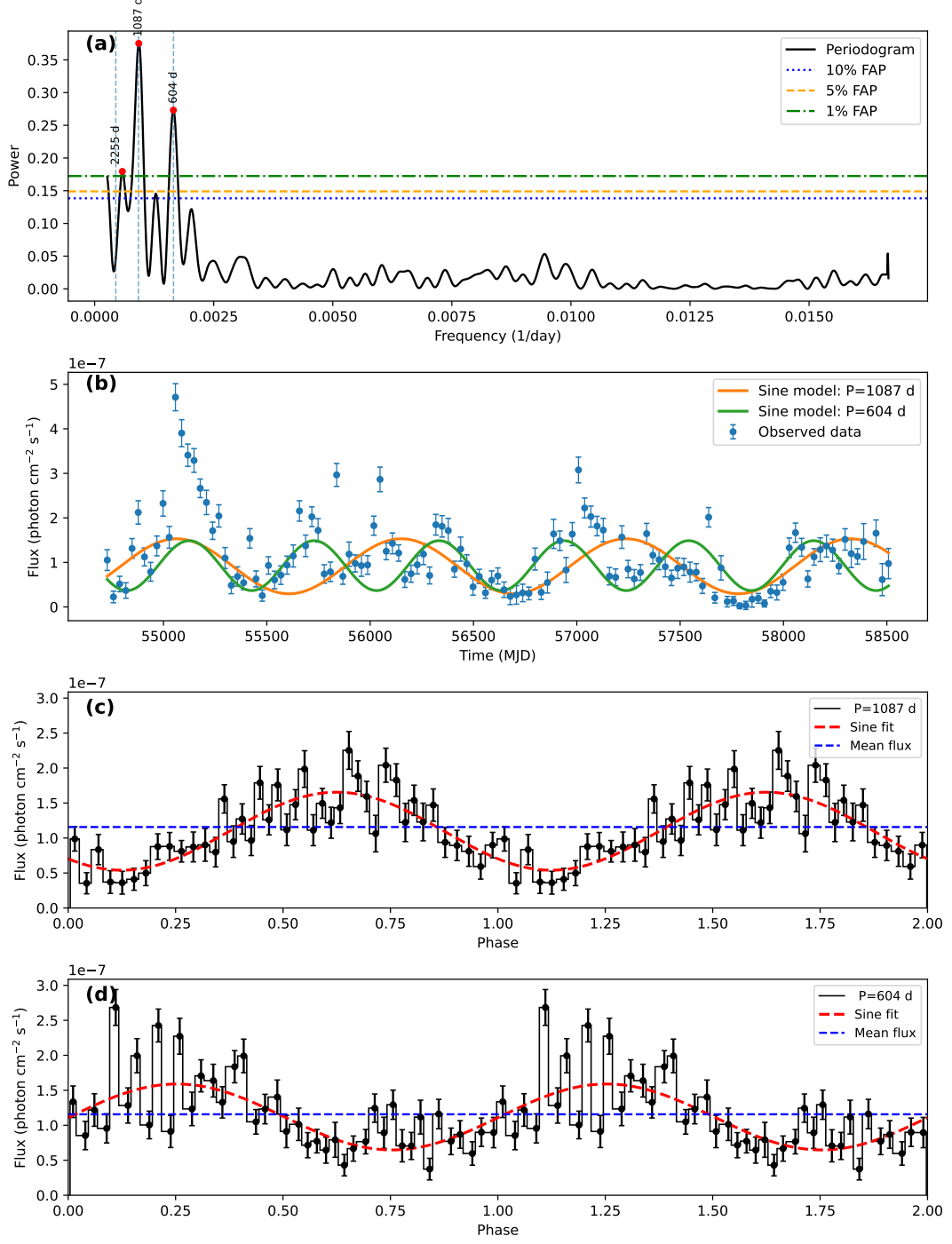


Figure 1: (a) LSP computed from the monthly binned *Fermi*-LAT data over MJD 54727.99–58507.99. The two most prominent peaks occur at frequencies of  $0.000920$  and  $0.001655$  day $^{-1}$ , corresponding to periods of  $P_1 = 1087.2 \pm 80.4$  d and  $P_2 = 604.2 \pm 23.4$  d, respectively. Horizontal lines mark the false-alarm-probability (FAP) levels of 10% (blue dotted), 5% (orange dashed), and 1% (green dash-dotted). (b)  $\gamma$ -ray light curve overlaid with the best-fitting sinusoidal models corresponding to the two LSP periods. (c,d) Phase-folded light curves for  $P_1$  and  $P_2$ , respectively, shown over two full cycles (phase 0–2). In each panel, the data points are plotted in black, the best-fit sinusoidal model is shown by the red dashed curve, and the horizontal blue dashed line indicates the mean flux level. The folding highlights the quasi-periodic modulation present in the  $\gamma$ -ray emission.

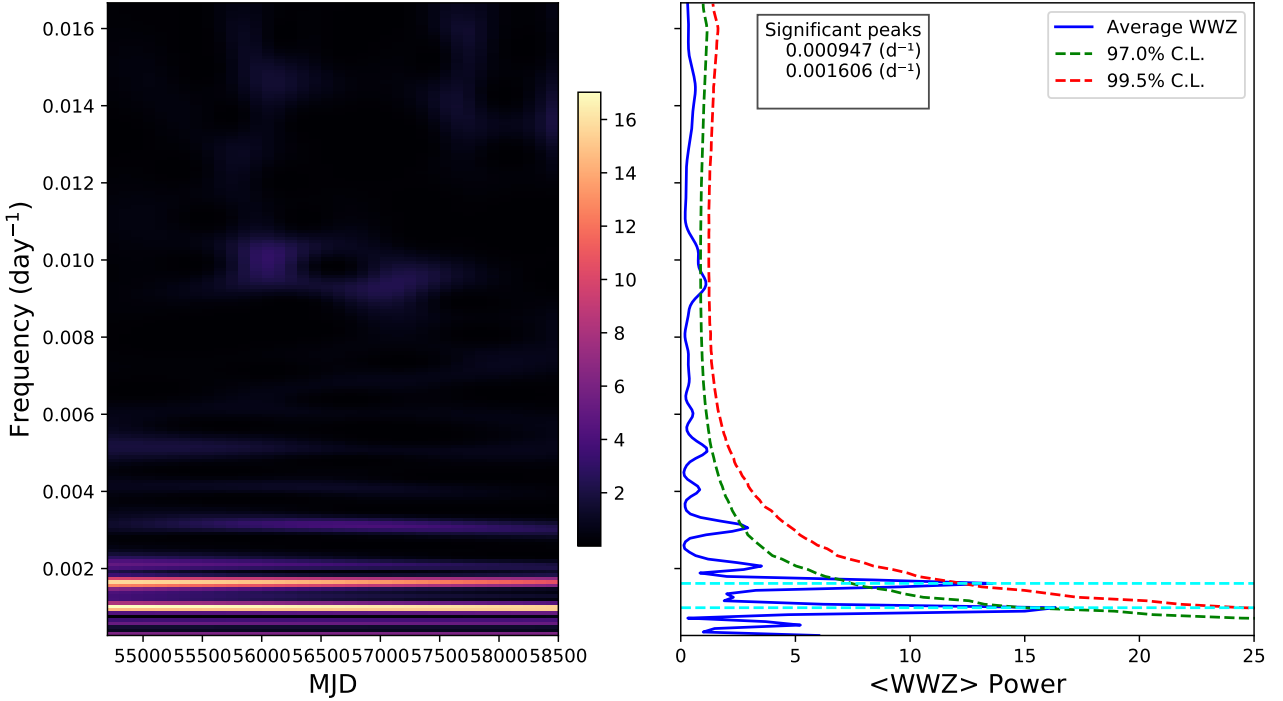
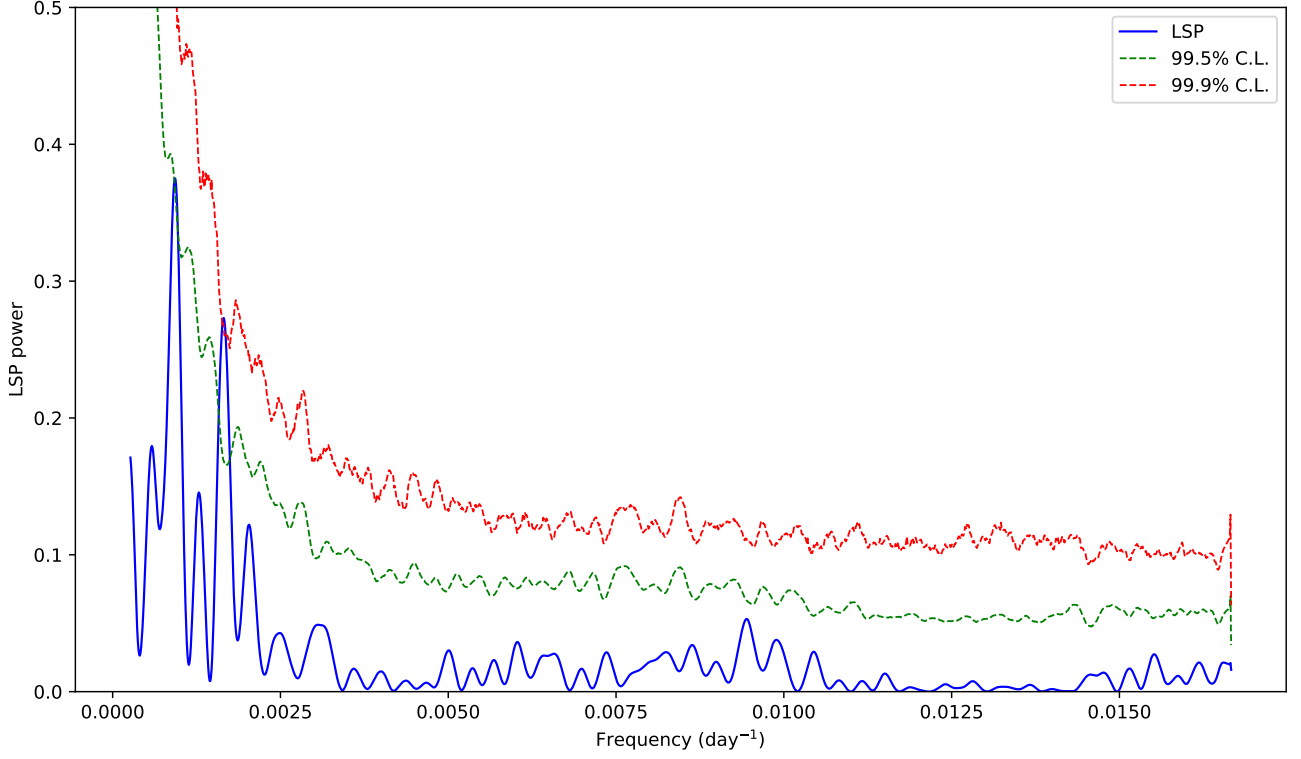


Figure 2: Top: LSP of the monthly binned  $\gamma$ -ray light curve of PKS 2052–47, showing two dominant peaks at frequencies of  $0.000920$  and  $0.001655$   $\text{d}^{-1}$  (periods of  $\sim 1087$  and  $\sim 604$  d), both exceeding the 99.5% confidence level derived from  $10^5$  Monte Carlo simulations following the method of Emmanoulopoulos et al. (2013). Bottom: Left: WWZ map of the  $\gamma$ -ray light curve showing the evolution of power as a function of time (MJD) and frequency. Right: The average WWZ power spectrum with confidence levels derived from  $10^5$  Monte Carlo simulations. The dashed green and red lines represent the 97.0% and 99.5% confidence levels, respectively. The dotted and dashed cyan lines mark the two most prominent peaks at frequencies of  $0.000947$  and  $0.001606$   $\text{day}^{-1}$ , corresponding to periods of  $\sim 1056$  and  $\sim 623$  d; the shorter-period feature exceeds the 99.5% level, while the longer-timescale peak reaches the  $\sim 97\%$  level.

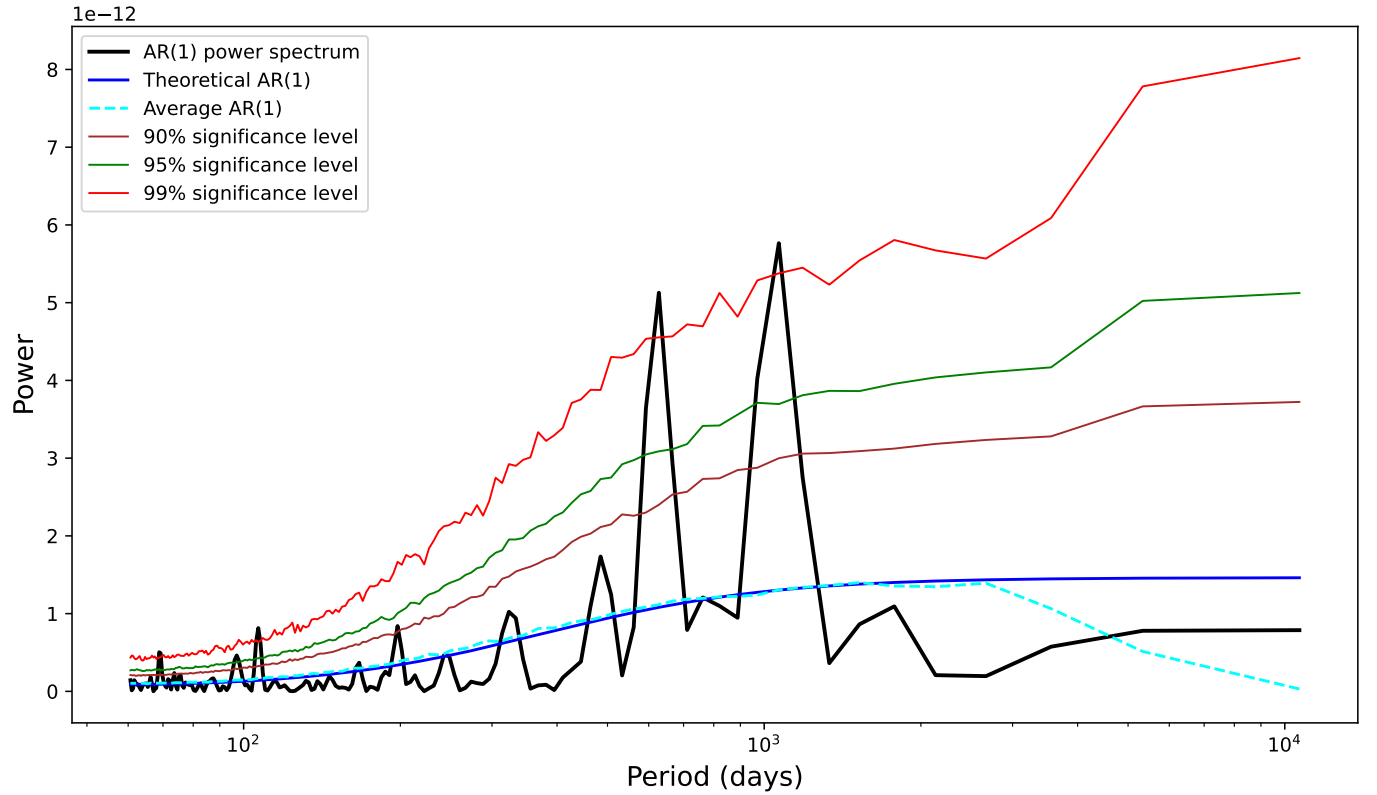


Figure 3: Red-noise-corrected REDFIT power spectrum of the  $\gamma$ -ray light curve of PKS 2052–47. The black curve shows the observed spectrum, while the blue and cyan curves correspond to the theoretical and ensemble-averaged AR(1) models, respectively. The brown, green, and red horizontal lines indicate the 90%, 95%, and 99% Monte Carlo confidence levels. Two dominant peaks are present, both exceeding the 99% significance threshold.

is the autoregressive coefficient associated with the characteristic timescale  $\tau$ , and  $\epsilon(t_i)$  denotes a random driving term. The corresponding theoretical power spectrum takes the form

$$G_{rr}(f_i) = G_0 \frac{1 - A^2}{1 - 2A \cos(\pi f_i / f_{\text{Nyq}}) + A^2}, \quad (3)$$

where  $G_0$  is the mean spectral power,  $f_i$  are the temporal frequencies, and  $f_{\text{Nyq}}$  denotes the Nyquist frequency.

The red-noise-corrected spectrum was computed using the REDFIT routine implemented in R<sup>4</sup>, and the statistical significance of candidate features was assessed via Equation (3). This procedure reveals two prominent peaks at  $0.000937 \pm 0.000101 \text{ d}^{-1}$  and  $0.00159 \pm 0.00012 \text{ d}^{-1}$ , corresponding to periods of approximately 1067 and 628 d, respectively; both exceed the 99% confidence level (see Figure 3). The uncertainties in the peak frequencies were estimated from the half-width at half-maximum (HWHM) of Gaussian fits to the REDFIT spectrum.

#### 3.4. Date-compensated Discrete Fourier Transform (DCDFT)

Estimating power spectra from unevenly sampled time series remains a central difficulty in the search for quasi-periodic oscillations in blazar light curves (e.g., Fan et al., 2007). When applied to such data, the classical discrete Fourier transform (DFT) can suffer from frequency shifts and amplitude distortions, which may compromise the reliability of detected periodic components. These effects are alleviated by the date-compensated discrete Fourier transform (DCDFT; Ferraz-Mello 1981; Foster 1995), which models the light curve through a least-squares fit that includes both sinusoidal and constant terms, rather than relying exclusively on purely sinusoidal components as in the standard DFT. This formulation is particularly advantageous at low frequencies ( $< 0.02 \text{ day}^{-1}$ ), where uneven sampling can otherwise introduce discrepancies of several per cent.

In our analysis, we applied the DCDFT to the  $\gamma$ -ray light curve using publicly available software<sup>5</sup>, which follows the formalism described by Ferraz-Mello (1981). The resulting modified periodogram  $H(\omega)$  exhibits two prominent peaks at  $0.00090 \pm 0.00015 \text{ d}^{-1}$  and  $0.00160 \pm 0.00020 \text{ d}^{-1}$ , corresponding to periods of  $\sim 1111$  and  $\sim 625$  d, respectively. Both features exceed the 99% confidence level (see Figure 4), indicating that they are statistically significant. Because the frequency grid in the DCDFT remains uniform regardless of data gaps, the method is well suited to long-term, irregularly sampled blazar monitoring.

The periodicities inferred from all four techniques are mutually consistent within uncertainties, with the shorter timescale emerging as the dominant modulation, as summarized in Table 1.

In this study, we report indication for a dominant quasi-periodic modulation in the  $\gamma$ -ray emission of PKS 2052–47 at a characteristic period of  $\sim 604$  d, together with a secondary longer-timescale feature near  $\sim 1087$  d inferred from the LSP. The shorter of the two timescales is consistently recovered by the WWZ, REDFIT, and DCDFT analyses, which yield periods in the range  $\sim 620$ – $628$  d, in close agreement with the  $\sim 642$  d modulation previously reported from weekly binned data by (Prokhorov and Moraghan, 2017).

#### 3.5. Damped Random Walk Model

The observed variability in AGN emission is stochastic in nature and can be well described by the simplest form of a continuous autoregressive moving average process, CARMA(1,0) (e.g., Moreno et al., 2019; Burke et al., 2021; Zhang et al., 2022, 2023; Sharma et al., 2024b; Tantry et al., 2025). This formulation is commonly referred to as the damped random walk (DRW) model and has been widely adopted to characterize red-noise variability in AGN light curves.

In this framework, the flux variations are governed by the stochastic differential equation

$$\left[ \frac{d}{dt} + \frac{1}{\tau_{\text{DRW}}} \right] y(t) = \sigma_{\text{DRW}} \epsilon(t), \quad (4)$$

where  $\tau_{\text{DRW}}$  denotes the characteristic damping timescale,  $\sigma_{\text{DRW}}$  is the long-term variability amplitude, and  $\epsilon(t)$  is a Gaussian white-noise process with zero mean and unit variance. The covariance function of the DRW process is given by

$$k(\Delta t) = \sigma_{\text{DRW}}^2 \exp\left(-\frac{|\Delta t|}{\tau_{\text{DRW}}}\right), \quad (5)$$

where  $\Delta t = |t_n - t_m|$  represents the time lag between two measurements.

The power spectral density (PSD) associated with the DRW model has the form of a broken power law,

$$S(\omega) = \sqrt{\frac{2}{\pi}} \frac{\sigma_{\text{DRW}}^2 \tau_{\text{DRW}}}{1 + (\omega \tau_{\text{DRW}})^2}, \quad (6)$$

where  $\omega$  is the angular frequency. At low frequencies ( $\omega \ll 1/\tau_{\text{DRW}}$ ), the PSD is approximately flat, while at high frequencies ( $\omega \gg 1/\tau_{\text{DRW}}$ ) it asymptotically approaches a  $P(\omega) \propto \omega^{-2}$  form, characteristic of red-noise dominated processes.

We modeled the  $\gamma$ -ray light curve of PKS 2052–47 using the publicly available EZTAO package<sup>6</sup>, which is built on top of the CELERITE Gaussian-process framework<sup>7</sup> (Foreman-Mackey et al., 2013). Parameter estimation was performed via Markov Chain Monte Carlo

<sup>4</sup><https://rdrr.io/cran/dplR/man/redfit.html>

<sup>5</sup><https://github.com/ilmimris/dcdft>

<sup>6</sup><https://eztao.readthedocs.io/en/latest/>

<sup>7</sup><https://celerite.readthedocs.io/en/stable/>

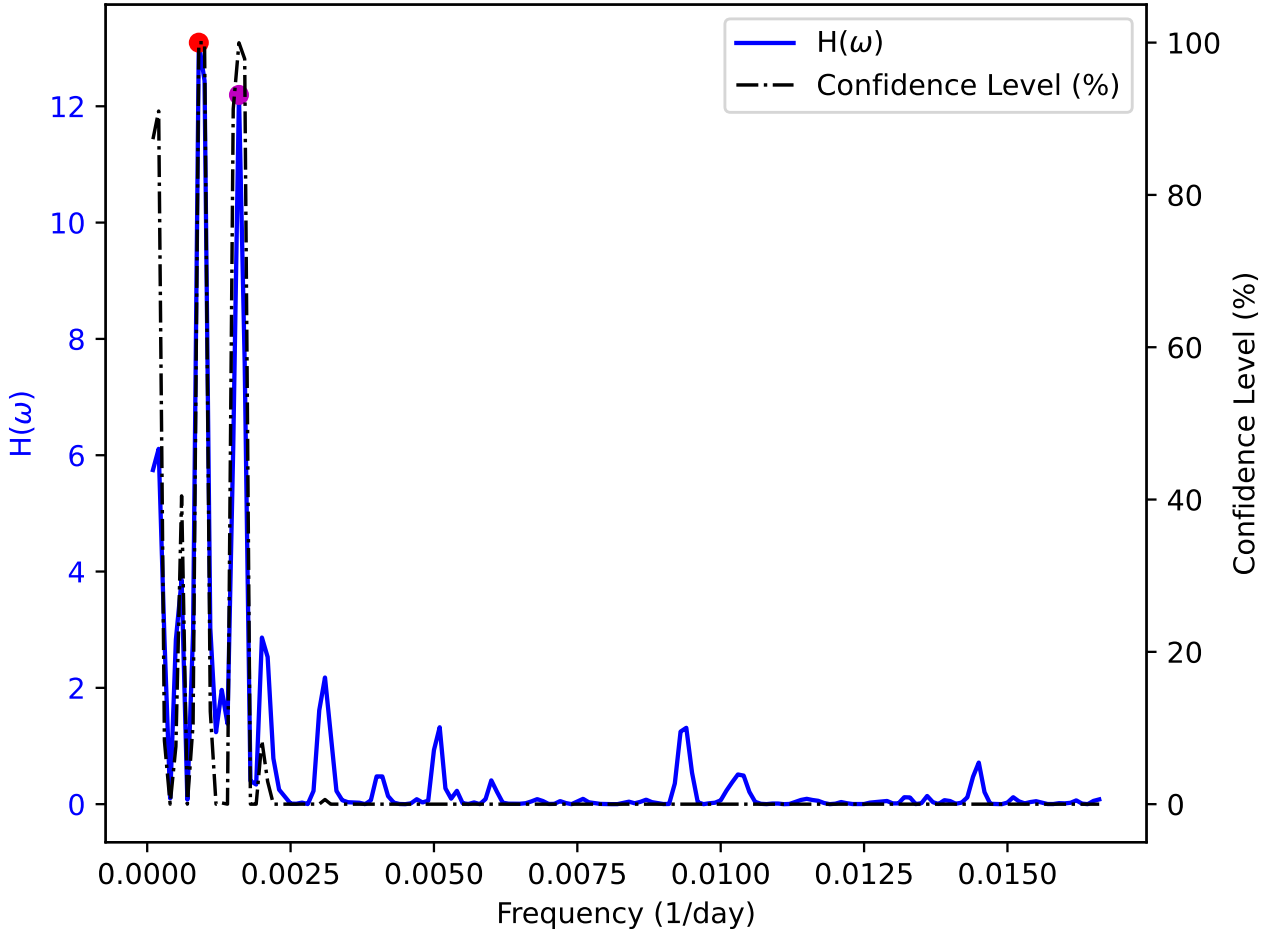


Figure 4: Modified periodogram  $H(\omega)$  obtained using the DCDFT method for the  $\gamma$ -ray light curve of PKS 2052–47. Two dominant peaks are detected at periods of  $\sim 1111$  and  $\sim 625$  d, consistent with the timescales inferred from the other timing techniques. The associated uncertainties were estimated by fitting Gaussian profiles to the corresponding features in the periodogram. The black dash-dotted curve denotes the 99% confidence level, which is exceeded by both peaks, indicating that they are statistically significant.

Table 1: Summary of QPO frequencies detected for PKS 2052–47 using different timing techniques. Uncertainties are quoted where available, and the local significance levels are given in parentheses. Frequencies are expressed in units of  $10^{-3}$  day $^{-1}$ .

4FGL Name	LSP ( $10^{-3}$ day $^{-1}$ )	WWZ ( $10^{-3}$ day $^{-1}$ )	REDFIT ( $10^{-3}$ day $^{-1}$ )	DCDFT ( $10^{-3}$ day $^{-1}$ )
4FGL J2056.2–4714	$0.920 \pm 0.068$ ( $> 99.5\%$ )	$0.947 \pm 0.100$ ( $> 97\%$ )	$0.937 \pm 0.101$ ( $> 99\%$ )	$0.900 \pm 0.150$ ( $> 99\%$ )
	$1.655 \pm 0.064$ ( $> 99.9\%$ )	$1.606 \pm 0.110$ ( $> 99.5\%$ )	$1.590 \pm 0.120$ ( $> 99\%$ )	$1.600 \pm 0.200$ ( $> 99\%$ )

(MCMC) sampling implemented using the `emcee` package<sup>8</sup> within EZTAO. In total, 25 000 MCMC realizations were generated, with the first 10 000 steps discarded as burn-in to ensure convergence of the chains. From the remaining samples, we derived the posterior distributions of the DRW model parameters and their associated uncertainties. The DRW power spectral densities derived from the maximum-likelihood solution and from the posterior-median parameters are shown in Figure 5. The solid curve corresponds to the PSD computed from the maximum-likelihood DRW parameters, while the dashed curve shows the PSD obtained using the posterior-median values from the MCMC sampling. Both spectra exhibit the characteristic low-frequency flattening and a steep high-frequency decline, consistent with the broken-power-law behaviour expected for a DRW process, with a break near  $f \sim 1/\tau_{\text{DRW}}$ . This feature corresponds to a characteristic stochastic timescale of  $\tau_{\text{DRW}} \approx 90$  d. The quasi-periodic modulation detected at  $\sim 600$ –630 d lies well beyond this timescale, indicating that it cannot be attributed to intrinsic DRW variability and instead requires an additional, non-stochastic component. The MCMC analysis yields median values of  $\ln \sigma_{\text{DRW}} = -16.35$  and  $\ln \tau_{\text{DRW}} = 4.55^{+0.33}_{-0.28}$  (with  $\tau_{\text{DRW}}$  in days), in excellent agreement with the maximum-likelihood estimates of  $\ln \sigma_{\text{DRW}} = -16.37$  and  $\ln \tau_{\text{DRW}} = 4.49$ . This close correspondence demonstrates that the DRW model provides a stable and statistically well-constrained description of the stochastic variability in the  $\gamma$ -ray light curve.

#### 4. Significance Evaluation

The red-noise variability commonly observed in AGN and blazar light curves is generally attributed to stochastic processes in the jet or accretion flow and can be described by a power-law power spectral density (PSD) of the form  $P(\nu) \propto A\nu^{-\beta}$ , where  $\nu$  denotes the temporal frequency and  $\beta > 0$  is the spectral index. For PKS 2052–47, Prokhorov and Moraghan (2017) reported a best-fitting PSD slope of  $\beta = 0.69$ . We adopted a Monte Carlo approach to quantify the statistical significance of the dominant peaks detected in the LSP and WWZ analyses. Specifically,  $10^5$  synthetic light curves were generated that reproduce both the power spectral density (PSD) and probability density function (PDF) of the observed data, following the prescription of Emmanoulopoulos et al. (2013). The local significance of each candidate feature was estimated from the distribution of spectral powers at the corresponding frequencies across the simulated realizations. Within the LSP analysis, the two principal peaks at  $\sim 0.000920$  d $^{-1}$  ( $\sim 1087$  d) and  $\sim 0.001655$  d $^{-1}$  ( $\sim 604$  d) both exceed the 99.5% confidence level. Consistent signals are recovered in the WWZ analysis, with peak frequencies clustered around  $\sim 0.001606$  d $^{-1}$  and

$\sim 0.000947$  d $^{-1}$ . The shorter-period signal exceeds the 99.5% confidence level, while the longer-timescale feature reaches the  $\sim 97\%$  confidence level in the average WWZ spectrum. The REDFIT results further support these detections, yielding dominant features near  $\sim 0.000937$  d $^{-1}$  and  $\sim 0.0016$  d $^{-1}$  with significance levels greater than 99%. Taken together, these findings provide indication for transient quasi-periodic modulations in the  $\gamma$ -ray light curve of PKS 2052–47 over the interval MJD 54727.99–58507.99, corresponding to approximately four and six modulation cycles for the longer and shorter timescales, respectively (see the panel (b) of Figure 2). In addition to the significance tests described above, we examined the  $\gamma$ -ray light curve using DRW framework, which is widely employed to characterize red-noise variability in AGN emission. The DRW-based significance testing and spectral-window analysis adopted here follow the methodology described in detail by (Tantry et al., 2025); we therefore provide only a concise summary and emphasize the elements specific to the present study. Using the EZTAO package, we generated 20,000 mock  $\gamma$ -ray light curves based on the maximum-likelihood DRW parameters inferred from the data and sampled them in an identical manner to the observed light curve. LSP were computed for each realization, and percentile thresholds corresponding to the  $1\sigma$ ,  $2\sigma$ ,  $3\sigma$ , and  $4\sigma$  confidence levels were derived at each trial frequency from the ensemble of simulations. We further constructed spectral-window periodograms to evaluate the impact of uneven sampling, following the procedure outlined by (Tantry et al., 2025). In this DRW-based framework, two prominent features near  $\sim 0.000920$  day $^{-1}$  and  $\sim 0.001655$  day $^{-1}$ —corresponding to periods of  $\sim 1087$  and  $\sim 604$  d—exceed the  $4\sigma$  confidence envelope. The corresponding DRW significance curves and spectral-window periodograms are shown in Figure 6.

#### 5. Temporal Evolution of the QPO

To assess the temporal persistence of the candidate QPOs at periods of 1087.2 and 604.2 d, we performed a sliding-window Lomb–Scargle analysis. In this method, the light curve was partitioned into overlapping temporal segments, within which the LSP power was evaluated at the two fixed periods. The resulting evolution of the LSP power, presented in Figure 7, shows that the strength of the signal changes over time. During several intervals the power rises above the 95th-percentile level, indicating that the oscillations are not present throughout the full data set but instead emerge episodically. This behaviour is typical of non-stationary or evolving QPOs and is compatible with scenarios in which the underlying physical process operates intermittently, potentially linked to time-variable conditions in the jet or accretion environment.

<sup>8</sup><https://github.com/dfm/emcee>

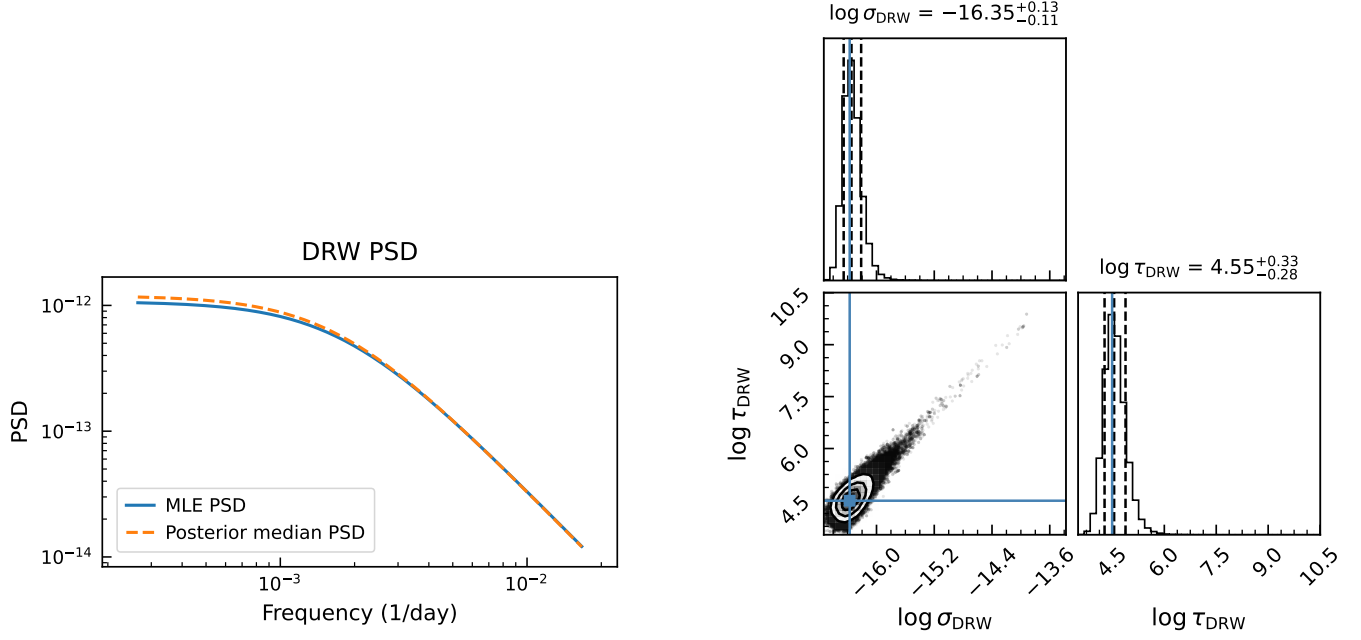


Figure 5: PSDs derived from the DRW modeling of the  $\gamma$ -ray light curve. *Left*: PSD obtained using the maximum-likelihood DRW parameters together with the posterior-median solution. *Right*: Corresponding PSD representation derived from the MCMC posterior samples. Both panels exhibit the characteristic low-frequency flattening and a steep high-frequency decline expected for a DRW process. The inferred parameters are  $\ln \sigma_{\text{DRW}} = -16.35$  and  $\ln \tau_{\text{DRW}} = 4.55^{+0.33}_{-0.28}$  (days), consistent with the maximum-likelihood values  $\ln \sigma_{\text{DRW}} = -16.37$  and  $\ln \tau_{\text{DRW}} = 4.49$ .

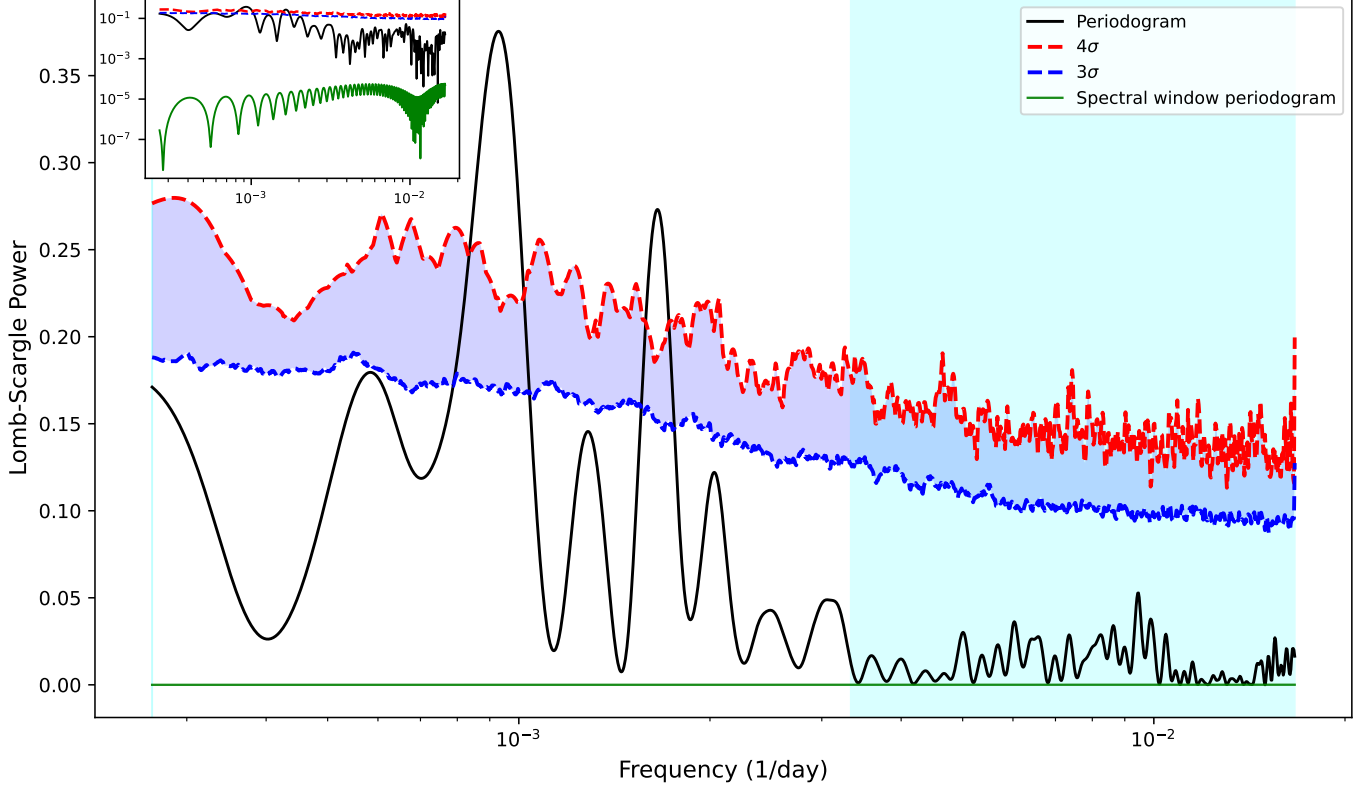


Figure 6: LSP of the monthly binned  $\gamma$ -ray light curve of PKS 2052–47 (black curve), together with the spectral-window periodogram (green) constructed to assess the effects of uneven temporal sampling. The dashed red curve shows the  $4\sigma$  significance threshold derived from 20 000 DRW simulations. Two dominant peaks near  $\sim 0.000920$  and  $\sim 0.001655$  day $^{-1}$  exceed this threshold, corresponding to periods of  $\sim 1087$  and  $\sim 604$  d, respectively. The cyan-shaded region marks the frequency range deemed unreliable owing to the finite duration of the light curve and cadence-based criteria adopted following (Tantry et al., 2025). The inset panel presents the same periodograms on logarithmic axes.

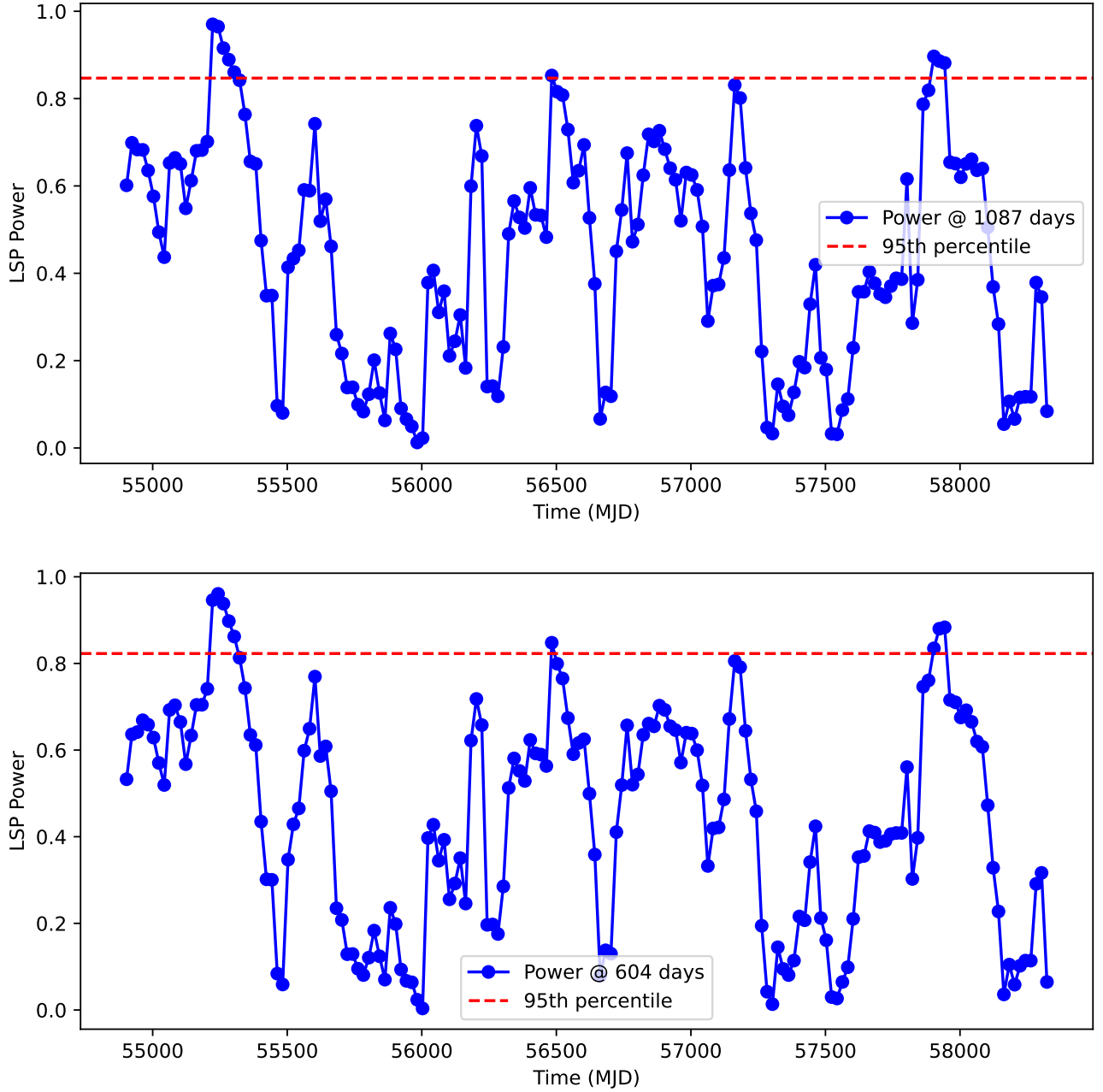


Figure 7: Windowed Lomb-Scargle power as a function of time at fixed periods of 1087.2 and 604.2 d. A sliding-window approach is used to trace the temporal evolution of the quasi-periodic signals across the full observational baseline. The horizontal dashed line marks the 95th-percentile significance threshold. Epochs in which the power exceeds this level indicate that the QPOs are intermittent and do not persist uniformly throughout the light curve.

## 6. Summary and Discussion

We conducted a systematic search for long-timescale QPOs in the  $\gamma$ -ray emission of the high-redshift FSRQ PKS 2052–47 using monthly binned *Fermi*-LAT data covering MJD 54727.99–58507.99. To minimise method-dependent biases and to account for uneven sampling and red-noise variability, we applied multiple, complementary timing techniques, including LSP, WWZ, REDFIT, and DCDFT. Our principal findings can be summarised as follows.

- Taken together, the multi-technique timing analyses reveal one dominant quasi-periodic modulation on a timescale of  $\sim 600$ –630 d and a secondary longer-timescale feature near  $\sim 1050$ –1110 d in the  $\gamma$ -ray light curve of PKS 2052–47.
- The LSP reveals prominent peaks at  $f \simeq 9.20 \times 10^{-4} \text{ d}^{-1}$  and  $f \simeq 1.66 \times 10^{-3} \text{ d}^{-1}$ , corresponding to  $P_1 \simeq 1087$  d and  $P_2 \simeq 604$  d. Phase-folded light curves at both periods show coherent modulations consistent with quasi-sinusoidal variability.
- The WWZ analysis independently detects signals at frequencies consistent with the LSP peaks and localises their power in time, indicating an evolving, non-stationary periodic component rather than a strictly persistent oscillation.
- Emmanoulopoulos-type Monte Carlo simulations that reproduce both the PSD and PDF of the observed light curve demonstrate that both candidate periods exceed the  $\gtrsim 99.5$  per cent local confidence levels in the LSP spectrum, while in the WWZ analysis the shorter-period signal exceeds this threshold and the longer-timescale feature reaches the  $\sim 97$  per cent confidence level.
- Independent red-noise modelling with a DRW framework yields a characteristic stochastic timescale of  $\tau_{\text{DRW}} \sim 90$  d. DRW-based simulations based on 20 000 realisations confirm that the QPO peaks exceed the  $4\sigma$  confidence envelope.
- Spectral-window diagnostics show that neither of the detected periodicities is produced by the sampling pattern of the data.
- A sliding-window LSP evaluated at fixed  $P_1$  and  $P_2$  demonstrates that the QPO power varies with time, with several intervals exceeding the 95th-percentile threshold and others falling below it, implying that the modulation is episodic rather than persistent across the full  $\sim 11$ -yr baseline.
- Over the  $\sim 11$  yr baseline, the number of observed cycles is approximately four for the longer timescale and six for the shorter.

### 6.1. Physical interpretation

Long-timescale QPOs in blazars continue to attract considerable interest because they may encode information about the dynamics of the central engine and the geometry of the relativistic jet. A wide range of physical scenarios has been proposed to explain year-scale or multi-year modulations in blazar light curves, including SMBBH systems, precession or helical motion of jets driven by geometric effects, and instabilities in the accretion flow that modulate plasma injection into the jet (e.g. Sillanpaa et al., 1988; Xie et al., 2008; Valtonen et al., 2008; Rieger, 2004; Gupta et al., 2008; Sandrinelli et al., 2016; Otero-Santos et al., 2020; Gong et al., 2022, 2024). Within this broader context, PKS 2052–47 represents a valuable new case study, as a dominant timescale near  $\sim 600$ –630 d and a secondary longer-timescale modulation near  $\sim 1050$ –1110 d are recovered independently by several timing techniques and are found to be statistically significant when tested against realistic red-noise models.

The coexistence of two characteristic periods, together with their episodic appearance in the sliding-window analysis, provides important clues to the underlying mechanism. In particular, the intermittency argues against a strictly coherent clock operating throughout the entire observing baseline and instead favours scenarios in which the physical driver becomes active only during specific epochs. Such behaviour is naturally produced in geometric models in which the jet orientation or the trajectory of a compact emitting region evolves quasi-periodically, thereby modulating the Doppler factor seen by the observer (e.g. Rieger, 2004; Villata and Raiteri, 1999; Otero-Santos et al., 2020; Sharma et al., 2024a). Even modest variations in the viewing angle can lead to pronounced flux swings in highly beamed sources, making Doppler-geometry effects particularly attractive for explaining long-term QPOs in  $\gamma$  rays.

Several specific geometric mechanisms may operate in PKS 2052–47. Jet precession driven by Lense–Thirring torques acting on a misaligned inner accretion flow provides one physically motivated channel for producing quasi-periodic changes in orientation (e.g. Rieger, 2004; Gupta et al., 2008). On longer timescales, torques exerted by a secondary black hole in a close SMBBH system can induce precession or nutation of the disc–jet system, leading to non-ballistic helical jet trajectories and periodic Doppler modulation (e.g. Sillanpaa et al., 1988; Valtonen et al., 2008; Gong et al., 2022, 2024). Alternatively, the emitting plasma may follow a rotating or helical path within a bent or twisted jet, giving rise to the classical “lighthouse” effect discussed in many earlier works (e.g. Villata and Raiteri, 1999; Rieger, 2004; Otero-Santos et al., 2020; Gong et al., 2023).

In these geometric pictures, the detection of two periods can be interpreted in several ways. One possibility is that the shorter timescale reflects a fundamental precession or pattern period, while the longer modulation corresponds to a commensurate or higher-order harmonic

activated during particular epochs. Another possibility is that the two timescales arise from distinct but coupled processes, such as simultaneous precession and nutation of the jet, thereby producing a beat-like envelope in the observed flux modulation. Similar near-harmonic structures have been reported in other blazars, where multiple year-scale periods were interpreted in terms of orbiting hot spots in the inner accretion disc or oscillatory modes triggered by Kelvin–Helmholtz instabilities that propagate into the jet (e.g. An et al., 2013; Otero-Santos et al., 2020; Gong et al., 2022). Although the ratio between  $P_2 \sim 600\text{--}630$  d and the longer modulation near  $\sim 1050\text{--}1110$  d is not an exact integer, the finite time baseline, red-noise contamination, and associated uncertainties leave open the possibility of a near-resonant relationship. The fact that the  $\sim 600\text{--}630$  d modulation is recovered by all methods, whereas the longer-timescale feature appears with lower or method-dependent significance, further supports this cautious interpretation.

Accretion-driven interpretations provide a complementary class of models and cannot be ruled out on the basis of  $\gamma$ -ray data alone. In such scenarios, oscillations in the innermost disc, magnetic-flux accumulation or reconnection cycles, or disc-wind interactions may modulate the rate at which energetic particles are injected into the jet, thereby imprinting quasi-periodic signatures that are subsequently amplified by relativistic beaming (e.g. Gupta et al., 2008; Bhatta et al., 2016; Tavani et al., 2018; Sandrinelli et al., 2016). Because multiple instability modes or emission zones may operate simultaneously, such intrinsic processes could also give rise to more than one characteristic timescale, consistent with the two periodicities reported here.

Despite the high statistical significance of the shorter  $\sim 600\text{--}630$  d period under red-noise-aware tests, and the more tentative nature of the longer modulation, their interpretation must be tempered by the finite observational window and the modest number of cycles sampled, particularly for the longer timescale. Similar cautions have been raised in several recent QPO studies, which emphasise that year-like periodicities in red-noise-dominated light curves can appear transient and require confirmation through continued monitoring (e.g. Sandrinelli et al., 2016; Otero-Santos et al., 2020; Gong et al., 2022). The episodic nature of the signals in PKS 2052–47 therefore highlights the importance of extending the temporal baseline and testing for recurrence in future *Fermi*-LAT data releases.

Looking ahead, a natural next step will be contemporaneous broadband SED modelling, which can constrain key physical parameters of the emission region, including the Doppler factor, characteristic electron energies, and source geometry. Such information is essential for evaluating specific geometric or binary-driven scenarios and for translating the observed QPO timescales into physically meaningful quantities. Complementary radio very-long-baseline interferometry could test for peri-

odic changes in jet position angle or recurrent component ejections, while optical polarimetric monitoring may uncover systematic electric-vector position-angle rotations associated with orientation changes in the emitting region. Together, these multiwavelength diagnostics would strongly discriminate between Doppler-geometry models and intrinsic dissipation scenarios and would ultimately enable attempts to connect the observed timescales to SMBBH-driven dynamics and to derive physically motivated constraints on the black-hole mass.

Although year-like QPOs in several blazars have been interpreted in terms of SMBBH-driven dynamics and used to place constraints on black-hole masses in the literature, we do not attempt such estimates here. Reliable mass inference requires adopting a specific physical model and independent constraints on the Doppler factor, viewing geometry, and binary mass ratio, which are beyond the scope of the present timing-focused analysis.

## 6.2. Conclusions

Taken together, the results presented here identify PKS 2052–47 as a promising new member of the small but growing class of blazars exhibiting long-timescale  $\gamma$ -ray QPOs. We find indication for a dominant quasi-periodic modulation on a timescale of  $\sim 600\text{--}630$  d, together with a secondary longer-timescale feature near  $\sim 1050\text{--}1110$  d. Their intermittent behaviour in sliding-window analyses, and their possible harmonic or near-resonant relationship, provide strong motivation for continued monitoring and for deeper theoretical modelling aimed at uncovering the physical origin of these oscillations.

Future progress will require coordinated multiwavelength campaigns, in particular contemporaneous broadband SED modelling to constrain key physical parameters of the emission region, together with radio VLBI and optical polarimetric observations to test Doppler-geometry scenarios and possible SMBBH-driven dynamics. Such efforts will be essential for establishing whether the detected modulations recur, for quantifying their duty cycle, and for determining whether they arise from geometric effects in the relativistic jet or from accretion-related instabilities at the jet base.

## 7. Acknowledgements

SAD express gratitude to the Inter-University Centre for Astronomy and Astrophysics (IUCAA) in Pune, India, for the support and facilities provided.

## References

Akbar, S., Shah, Z., Misra, R., Boked, S., Iqbal, N., 2025. Indication for dual periodic signatures in pks 0805-07 from multitechnique time series analysis. Phys. Rev. D 112, 063061. URL: <https://link.aps.org/doi/10.1103/zxgfv-fzv5>, doi:10.1103/zxgfv-fzv5.

An, T., Baan, W.A., Wang, J.Y., Wang, Y., Hong, X.Y., 2013. Periodic radio variabilities in nrao 530: a jet-disc connection? *Monthly Notices of the Royal Astronomical Society* 434, 3487–3496.

Atwood, W.B., Abdo, A.A., Ackermann, M., Althouse, W., Anderson, B., Axelsson, M., Baldini, L., Ballet, J., Band, D.L., Barbierini, G., Bartelt, J., Bastieri, D., Baughman, B.M., Bechtol, K., Bédérède, D., Bellardi, F., Bellazzini, R., Berenji, B., Bignami, G.F., Bisello, D., Bissaldi, E., Blandford, R.D., Bloom, E.D., Bogart, J.R., Bonamente, E., Bonnell, J., Borgland, A.W., Bouvier, A., Bregeon, J., Brez, A., Brigida, M., Bruel, P., Burnett, T.H., Busetto, G., Caliandro, G.A., Cameron, R.A., Caraveo, P.A., Carius, S., Carlson, P., Casandjian, J.M., Cavazzuti, E., Ceccanti, M., Cecchi, C., Charles, E., Chekhtman, A., Cheung, C.C., Chiang, J., Chipaux, R., Cillis, A.N., Ciprini, S., Claus, R., Cohen-Tanugi, J., Condamoor, S., Conrad, J., Corbet, R., Corucci, L., Costamante, L., Cutini, S., Davis, D.S., Decotigny, D., DeKlotz, M., Dermer, C.D., de Angelis, A., Digel, S.W., do Couto e Silva, E., Drell, P.S., Dubois, R., Dumora, D., Edmonds, Y., Fabiani, D., Farnier, C., Favuzzi, C., Flath, D.L., Fleury, P., Focke, W.B., Funk, S., Fusco, P., Gargano, F., Gasparini, D., Gehrels, N., Gentit, F.X., Germani, S., Giebels, B., Giglietto, N., Giommi, P., Giordano, F., Glanzman, T., Godfrey, G., Grenier, I.A., Grondin, M.H., Grove, J.E., Guillemot, L., Guiriec, S., Haller, G., Harding, A.K., Hart, P.A., Hays, E., Healey, S.E., Hirayama, M., Hjalmarsdotter, L., Horn, R., Hughes, R.E., Jóhannesson, G., Johansson, G., Johnson, A.S., Johnson, R.P., Johnson, T.J., Johnson, W.N., Kamae, T., Katagiri, H., Kataoka, J., Kavelaars, A., Kawai, N., Kelly, H., Kerr, M., Klamra, W., Knödlseder, J., Kocian, M.L., Komin, N., Kuehn, F., Kuss, M., Landriu, D., Latronico, L., Lee, B., Lee, S.H., Lemoine-Goumard, M., Lionetto, A.M., Longo, F., Loparco, F., Lott, B., Lovellette, M.N., Lubrano, P., Madejski, G.M., Makeev, A., Marangelli, B., Massai, M.M., Mazzotta, M.N., McEnery, J.E., Menon, N., Meurer, C., Michelson, P.F., Minuti, M., Mirizzi, N., Mithumsiri, W., Mizuno, T., Moiseev, A.A., Monte, C., Monzani, M.E., Moretti, E., Morselli, A., Moskalenko, I.V., Murgia, S., Nakamori, T., Nishino, S., Nolan, P.L., Norris, J.P., Nuss, E., Ohno, M., Ohsugi, T., Omodei, N., Orlando, E., Ormes, J.F., Paccagnella, A., Panque, D., Panetta, J.H., Parent, D., Pearce, M., Pepe, M., Perazzo, A., Pesce-Rollins, M., Picozza, P., Pieri, L., Pinchera, M., Piron, F., Porter, T.A., Poupart, L., Rainò, S., Rando, R., Rapposelli, E., Razzano, M., Reimer, A., Reimer, O., Reposeur, T., Reyes, L.C., Ritz, S., Rochester, L.S., Rodriguez, A.Y., Romani, R.W., Roth, M., Russell, J.J., Ryde, F., Sabatini, S., Sadrozinski, H.F.W., Sanchez, D., Sander, A., Sapozhnikov, L., Parkinson, P.M.S., Scargle, J.D., Schalk, T.L., Scolieri, G., Sgrò, C., Share, G.H., Shaw, M., Shimokawabe, T., Shrader, C., Sierpowska-Bartosik, A., Siskind, E.J., Smith, D.A., Smith, P.D., Spandre, G., Spinelli, P., Starck, J.L., Stephens, T.E., Strickman, M.S., Strong, A.W., Suson, D.J., Tajima, H., Takahashi, H., Takahashi, T., Tanaka, T., Tenze, A., Tether, S., Thayer, J.B., Thayer, J.G., Thompson, D.J., Tibaldo, L., Tibolla, O., Torres, D.F., Tosti, G., Tramacere, A., Turri, M., Usher, T.L., Vilchez, N., Vitale, V., Wang, P., Watters, K., Winer, B.L., Wood, K.S., Ylinen, T., Ziegler, M., 2009. The Large Area Telescope on the Fermi Gamma-Ray Space Telescope Mission. *Astrophys. J.* 697, 1071–1102. doi:10.1088/0004-637X/697/2/1071, arXiv:0902.1089.

Baluev, R.V., 2008. Assessing the statistical significance of periodogram peaks. *Mon. Not. R. Astron. Soc.* 385, 1279–1285. doi:10.1111/j.1365-2966.2008.12689.x, arXiv:0711.0330.

Bhatta, G., Zola, S., Ostrowski, M., Winiarski, M., Ogloza, W., Drózdź, M., Siwak, M., Liakos, A., Kozieł-Wierzbowska, D., Gazeas, K., et al., 2016. Detection of possible quasi-periodic oscillations in the long-term optical light curve of the bl lac object oj 287. *The Astrophysical Journal* 832, 47.

Boeck, M., Kadler, M., Tosti, G., Burnett, T., Ojha, R., Mueller, C., Wilms, J., 2009. Extragalactic Jets from the TANAMI Sample as Seen by Fermi/LAT. arXiv e-prints, arXiv:0912.4192doi:10.48550/arXiv.0912.4192, arXiv:0912.4192.

Burke, C.J., Shen, Y., Blaes, O., Gammie, C.F., Horne, K., Jiang, Y.F., Liu, X., McHardy, I.M., Morgan, C.W., Scaringi, S., et al., 2021. A characteristic optical variability time scale in astrophysical accretion disks. *Science* 373, 789–792.

Buson, S., Angioni, R., 2020. Fermi-LAT detection of enhanced gamma-ray activity from the FSRQ PKS 2052-47. *The Astronomer's Telegram* 13541, 1.

Chang, C.S., 2009. Fermi LAT detection of increasing gamma-ray activity of blazar PKS 2052-474. *The Astronomer's Telegram* 2160, 1.

Chang, C.S., Ros, E., Kadler, M., Ojha, R., the Fermi Lat Collaboration, the Tanami Team, the F-Gamma Team, 2010. Multiwavelength campaign of the gamma-ray flaring source PKS 2052-47. arXiv e-prints, arXiv:1001.1563doi:10.48550/arXiv.1001.1563, arXiv:1001.1563.

Emmanoulopoulos, D., McHardy, I., Papadakis, I., 2013. Generating artificial light curves: revisited and updated. *Monthly Notices of the Royal Astronomical Society* 433, 907–927.

Fan, J.H., Liu, Y., Yuan, Y., Hua, T., Wang, H., Wang, Y., Yang, J., Gupta, A., Li, J., Zhou, J., et al., 2007. Radio variability properties for radio sources. *Astronomy & Astrophysics* 462, 547–552.

Ferraz-Mello, S., 1981. Estimation of periods from unequally spaced observations. *ASTRONOMICAL JOURNAL* V. 86, P. 619, 1981 86, 619.

Foreman-Mackey, D., Hogg, D.W., Lang, D., Goodman, J., 2013. emcee: The MCMC Hammer. *Publ. Astron. Soc. Pac.* 125, 306. doi:10.1086/670067, arXiv:1202.3665.

Foster, G., 1995. The cleanest fourier spectrum. *The Astronomical Journal* (ISSN 0004-6256), vol. 109, no. 4, p. 1889-1902 109, 1889–1902.

Foster, G., 1996. Wavelets for period analysis of unevenly sampled time series. *Astronomical Journal* v. 112, p. 1709-1729 112, 1709–1729.

Gong, Y., Gao, Q., Li, X., Yuan, M., Yi, T., Li, H., Qin, L., Yang, H., Yang, H., Zhang, P., et al., 2024. The detection of possible quasiperiodic oscillations in the bl lac 4fgl j2139. 4- 4235. *The Astrophysical Journal* 976, 51.

Gong, Y., Tian, S., Zhou, L., Yi, T., Fang, J., 2023. Two transient quasi-periodic oscillations in  $\gamma$ -ray emission from the blazar s4 0954+ 658. *The Astrophysical Journal* 949, 39.

Gong, Y., Zhou, L., Yuan, M., Zhang, H., Yi, T., Fang, J., 2022. Quasiperiodic behavior in the  $\gamma$ -ray light curve of the blazar pks 0405-385. *The Astrophysical Journal* 931, 168.

Gupta, A.C., Srivastava, A., Wiita, P.J., 2008. Periodic oscillations in the intra-day optical light curves of the blazar s5 0716+ 714. *The Astrophysical Journal* 690, 216.

Hauser, M., Behera, B., Hagen, H., Wagner, S., 2009. Detection of an optical flare from PKS 2052-474. *The Astronomer's Telegram* 2158, 1.

Jauncey, D.L., Batty, M.J., Wright, A.E., Peterson, B.A., Savage, A., 1984. Redshifts of southern radio sources. VI. *Astrophys. J.* 286, 498–502. doi:10.1086/162624.

Kadler, M., Ojha, R., Tingay, S., Lovell, J., TANAMI Collaboration, 2007. The TANAMI Program: Southern-Hemisphere VLBI Monitoring of Relativistic Jets in Active Galaxies, in: American Astronomical Society Meeting Abstracts, p. 04.13.

Lomb, N.R., 1976. Least-squares frequency analysis of unequally spaced data. *Astrophysics and space science* 39, 447–462.

Marshall, H.L., Schwartz, D.A., Lovell, J.E.J., Murphy, D.W., Worrall, D.M., Birkinshaw, M., Gelbord, J.M., Perlman, E.S., Jauncey, D.L., 2005. A chandra survey of quasar jets: First results. *The Astrophysical Journal Supplement Series* 156, 13. URL: <https://doi.org/10.1086/425578>, doi:10.1086/425578.

Moreno, J., Vogeley, M.S., Richards, G.T., Yu, W., 2019. Stochastic modeling handbook for optical agn variability. *Publications of the Astronomical Society of the Pacific* 131, 063001.

Nazir, Z., Akbar, S., Shah, Z., Dar, A.A., Malik, Z., 2026. Broadband Variability Analysis of FSRQ PKS\0402-362 with Indications of Quasi-Periodic Modulation. arXiv e-prints, arXiv:2601.13181doi:10.48550/arXiv.2601.13181, arXiv:2601.13181.

Otero-Santos, J., Acosta-Pulido, J., Becerra González, J., Raiteri, C.M., Larionov, V., Peñil, P., Smith, P., Ballester Niebla, C., Borman, G., Carnerero, M., et al., 2020. Quasi-periodic behaviour in the optical and  $\gamma$ -ray light curves of blazars 3c 66a and b2 1633+ 38. *Monthly Notices of the Royal Astronomical Society* 492, 5524–5539.

Prokhorov, D.A., Moraghan, A., 2017. A search for cyclical sources of  $\gamma$ -ray emission on the period range from days to years in the Fermi-LAT sky. *Mon. Not. R. Astron. Soc.* 471, 3036–3042. doi:10.1093/mnras/stx1742, arXiv:1707.05829.

Rieger, F.M., 2004. On the geometrical origin of periodicity in blazar-type sources. *The Astrophysical Journal* 615, L5.

Sandrinelli, A., Covino, S., Dotti, M., Treves, A., 2016. Quasi-

periodicities at year-like timescales in blazars. *The Astronomical Journal* 151, 54.

Scargle, J.D., 1982. Studies in astronomical time series analysis. ii-statistical aspects of spectral analysis of unevenly spaced data. *Astrophysical Journal, Part 1*, vol. 263, Dec. 15, 1982, p. 835-853. 263, 835-853.

Schulz, M., Mudelsee, M., 2002. Redfit: estimating red-noise spectra directly from unevenly spaced paleoclimatic time series. *Computers & Geosciences* 28, 421-426.

Sharma, A., Banerjee, A., Das, A.K., Mandal, A., Bose, D., 2024a. Detection of a transient quasiperiodic oscillation in  $\gamma$ -rays from blazar pks 2255-282. *The Astrophysical Journal* 975, 56.

Sharma, A., Prince, R., Bose, D., 2024b. Microquasars to agns: An uniform jet variability. *arXiv preprint arXiv:2410.06653*.

Sillanpää, A., Haarala, S., Valtonen, M., Sundelius, B., Byrd, G., 1988. Oj 287-binary pair of supermassive black holes. *Astrophysical Journal, Part 1* (ISSN 0004-637X), vol. 325, Feb. 15, 1988, p. 628-634. Research supported by Nordisk Institut for Teoretisk Atomfysik and NSF. 325, 628-634.

Tantry, J., Sharma, A., Shah, Z., Iqbal, N., Bose, D., 2025. Study of multi-wavelength variability, emission mechanism and quasi-periodic oscillation for transition blazar s5 1803+784. *Journal of High Energy Astrophysics* 47, 100372. URL: <https://www.sciencedirect.com/science/article/pii/S2214404825000539>, doi:<https://doi.org/10.1016/j.jheap.2025.100372>.

Tavani, M., Cavalieri, A., Munar-Adrover, P., Argan, A., 2018. The blazar pg 1553+ 113 as a binary system of supermassive black holes. *The Astrophysical Journal* 854, 11.

Valtonen, M.J., Lehto, H., Nilsson, K., Heidt, J., Takalo, L., Sillanpää, A., Villforth, C., Kidger, M., Poyner, G., Pursimo, T., et al., 2008. A massive binary black-hole system in oj 287 and a test of general relativity. *Nature* 452, 851-853.

VanderPlas, J.T., 2018. Understanding the lomb-scargle periodogram. *The Astrophysical Journal Supplement Series* 236, 16.

Villata, M., Raiteri, C., 1999. Helical jets in blazars. i. the case of mkn 501. *Astronomy and Astrophysics*, v. 347, p. 30-36 (1999) 347, 30-36.

Wood, M., Caputo, R., Charles, E., Di Mauro, M., Magill, J., Perkins, J.S., Fermi-LAT Collaboration, 2017. Fermipy: An open-source Python package for analysis of Fermi-LAT Data, in: 35th International Cosmic Ray Conference (ICRC2017), p. 824. doi:[10.22323/1.301.0824](https://doi.org/10.22323/1.301.0824), arXiv:1707.09551.

Xie, G., Yi, T., Li, H., Zhou, S., Chen, L., 2008. Periodicity analysis of the radio curve of pks 1510-089 and implications for its central structure. *The Astronomical Journal* 135, 2212.

Zhang, H., Yan, D., Zhang, L., 2022. Characterizing the  $\gamma$ -ray variability of active galactic nuclei with the stochastic process method. *The Astrophysical Journal* 930, 157.

Zhang, H., Yan, D., Zhang, L., 2023. Gaussian process modeling blazar multiwavelength variability: Indirectly resolving jet structure. *The Astrophysical Journal* 944, 103.

## 8. Appendix